31p

X64 10363

Code 2A

VIBRATION STUDIES ON A SIMPLIFIED 1/2-SCALE MODEL OF THE NIMBUS SPACECRAFT

By Huey D. Carden and Robert W. Herr [1963] 31p & refs

NASA Langley Research Center,
Langley Station, ~~Hampton,~~ Va.

☐ cy

Presented at the 33rd ~~Symposium~~ on Shock, Vibration, and ~~Associated~~ Environments, Washington, ~~D.C.~~ December 3-5, 1963

(NASA TM X-51197)

VIBRATION STUDIES ON A SIMPLIFIED 1/2-SCALE MODEL OF THE NIMBUS SPACECRAFT

By Huey D. Carden* and Robert W. Herr*

INTRODUCTION

The high reliability demanded of spacecraft requires that these complex structures be capable of operation during and after exposure to many hostile environments. Earliest of the flight environmental hazards encountered, and in many cases the most severe, are the extreme vibration levels through which these payloads pass during the launch and boost phases of the flight sequence.

At the present time, onboard instrumentation of a variety of spacecraft is being designed and developed to operate on power generated by solar cells mounted on large flexible panels. Vibration tests of prototype spacecraft of this type, at levels well below anticipated flight levels, have resulted in damage to the payloads and instrumentation. It is anticipated that future payloads of like design will experience similar vibration problems; therefore, it becomes necessary that means and techniques be explored for reducing the severity of the many resonant conditions which exist in the spacecraft and its component parts.

The purpose of this paper is to present the results of an experimental investigation which utilized a 1/2-scale dynamic model of a spacecraft typical of the solar panel category for evaluating the effectiveness of damping and isolation in reducing the dynamic response of the spacecraft to vibratory inputs.

*Aerospace Engineers.

DISCUSSION

Description of model.- The configuration of the half-scale model utilized is shown in figure 1. The model was a simplified version of the full-scale Nimbus weather satellite. The bending stiffness of the solar panels, panel shaft, and struts as well as the mass of the major components in the model were approximately scaled. Two sets of simulated solar panels were fabricated. Both consisted of two sheets of 0.016-inch aluminum attached to a tapered balsa wood core. The taper of the wood core from the center of the panel along the length to the panel tips made it possible to obtain the desired stiffness distribution. In one set the aluminum sheets were bonded to the wood core with an epoxy cement, while in the other set the sheets were bonded with a viscoelastic adhesive to provide shear damping. The principal dimensions of the components of the 1/2-scale Nimbus model are presented in figure 2.

Test procedure.- For tests involving excitation along the pitch and roll axes, the 1/2-scale model was mounted on a platform which was suspended on steel flexure springs to provide essentially planar motions. For excitation along the yaw axis the model was suspended by nylon ropes attached at the center of gravity of the control section, struts and solar panels combination, and at the center of gravity of the sensory system - adapter combination. Excitation of the model was provided by an electromagnetic shaker. Input accelerations and the response of the model were measured with lightweight accelerometers while the excitation frequency was measured by a frequency-period counter. Responses of the model to input accelerations along the roll, pitch, or yaw axis were measured on the solar panels, control section, and sensory section for the basic model configuration and for cases for which damping and/or isolation had been incorporated in the structure.

ANALYTICAL AND EXPERIMENTAL RESULTS

Panel frequencies and mode shapes.- Concurrent with the experimental determination of the structural amplification factors of the 1/2-scale Nimbus model, an analytical technique for calculating the modes and frequencies of the simulated solar panels was employed. The technique utilizes a general finite-difference method for calculating the simple harmonic flexures of plates. The basis of the technique along with the procedure for application of the method to plate vibration problems is discussed fully in NASA TN D-536 (ref. 1). Additional information needed for calculating the modes and frequencies of the simulated solar panels using the technique is included in an appendix.

Computed frequencies and node locations for the first 10 modes are compared with experimental results in figure 3 where it can be seen that the agreement, in general, is good. The largest discrepancies occurred for modes four, five, and six. Closer correspondence between all computed and experimental frequencies could possibly be realized by more sophisticated assumptions on the edge conditions, more refined panel stiffness distribution for input into the computing machine procedure, and taking panel-cutouts into consideration.

The dashed lines in figure 3 indicate the computed node lines for the panel considered as completely rectangular in form. The actual planform, however, had panel cutouts as indicated by the small shaded areas at three corners. Substantial agreement, nevertheless, is shown between computed and experimental (solid lines) nodes.

Comparison of model response to full-scale vehicle response.- In order to assess the degree of simulation obtained with the 1/2-scale dynamic model of Nimbus, a comparison between the 1/2-scale model response and the response of the full-scale spacecraft was made at the base of the control assembly for input

along the pitch axis. In figure 4 the 1/2-scale model response is given by the dashed line and open symbols - the solid symbols denote the peak values of the measured resonance. Input accelerations to the model were limited by the available shaker force to approximately 83 percent of the desired 0.6g input level. Shown in the figure as a solid line is the corresponding experimentally measured full-scale vehicle response.[1]

The figure shows that general agreement exists between the model and full-scale vehicle resonances in the frequency range up to approximately 35 cps. However, two low-frequency resonant responses were measured on the 1/2-scale model which were not noted on the full-scale Nimbus. It is probable that the compromises and trade-offs necessitated in the construction of the model struts and strut attachments may have introduced these additional responses. But it is also possible that the inherent damping in these modes on the full-scale spacecraft was sufficiently high to mask out the individual modal responses.

In an elastic structure the response of the structure is dependent on the input accelerations and the amplification factors which relate the response of the structure to the input accelerations. For the 1/2-scale model under consideration, the primary interest was the determination of the amplification factors for the spacecraft and the evaluation of the effectiveness of certain damping and isolation techniques for attenuating these amplifications.

Effects of damping.- One of the more significant elements affecting the amplification factors is the damping of the structure. In general, any increase

---

[1]These data were supplied by the Goddard Space Flight Center and were obtained during Nimbus vibration analysis performed by the General Electric Co., Missile and Space Vehicle Department, Valley Forge, Pa., under contract to Goddard.

in the damping of the structure is beneficial but the use of damping can be made more effective by distribution of viscoelastic materials in areas of maximum relative shear displacement between two sandwich faces (ref. 2). Thus for minimum structural response to a given input spectrum, every attempt should be made to incorporate damping in the structure and to distribute the damping in areas as indicated by the critical modes.

The results of the study of the effects of distributed damping in the solar panels of the 1/2-scale model are given in figures 5 and 6. The measured damping, expressed as C/C_c, for the epoxy cement bonded panels and the damping adhesive bonded panels was approximately 0.003 and 0.020, respectively, for the first mode of the panel. In figures 5(a) to 5(d) amplification factors are given as a function of excitation frequency for locations and directions as indicated by the arrows on the inserted sketch of the model. Excitation in each case was along the roll axis, and the spring stiffness between the control section and the sensory section was $k = 15{,}250$ lb/in. Figures 6(a) to 6(c) present amplification factors for the case of excitation along the pitch axis at three of the same locations as those chosen for the cases in the roll direction. The test results shown in the figures emphasize three significant points. The first is that very high amplifications exist in such structures. Values as high as 30, 40, or 50 may be noted on the panels for the locations indicated. Secondly, the many structural resonances were associated mainly with panel natural modes. This suggests that proper design of the solar panels may be a means of locating the natural frequencies of the structure in certain areas of the frequency spectrum. In this manner significant reductions in conditions of resonance between the spacecraft panels and the booster inputs may be feasible. The third point is that the response of such a structure to unsteady forces can be substantially reduced, in most

instances, by the use of damping materials at suitably chosen points. A comparison of the levels of the solid curves to the dashed curves in figures 5 and 6 indicates the relatively high degree of energy dissipation that was attained in the sandwich construction panels. The added damping was least effective at the base of the control section, particularly for excitation along the roll axis (fig. 5(d)).

Effects of isolation and damping.- As an additional phase of the investigation of the 1/2-scale Nimbus model, a study of the effects of a combination of isolation and damping on the response of the vehicle to vibratory inputs was conducted. Commercially available isolators were utilized at the strut attachment points during the tests. The effective maximum radial capacity of the combination was experimentally determined as approximately $15\frac{1}{2}$ pounds. Two mounts had radial load capacities of $12\frac{1}{2}$ pounds each and the other had a radial load capacity of 20 pounds maximum. Typical results of the tests are presented in figure 7 for excitation along the pitch axis for which both damping and isolation were utilized. The results indicate that the isolation mounts were more effective in reducing the magnitudes of structural amplifications of the epoxy bonded panels than the inherently damped sandwich panels. The combination of both isolation mounts and the damping adhesive bonded panels was extremely effective in reducing the magnitude of detectable structural amplifications.

For excitation along the yaw axis, amplification factors were determined for locations on the base of the control section and on the bottom center of the solar panel. The response of the model for a spring stiffness between the control and sensory section of $k = 60{,}000$ lb/in. was used for comparison with the response for cases in which the isolation mounts were used. The results of these tests are presented in figure 8. For the location on the control section

(fig. 8(a)), the amplification factors as a function of frequency were the typical mass-on-isolator response curve with attenuation occurring at frequencies above approximately 1.4 times the natural frequency of the mass-isolator system. As shown in figure 8(a), the measured attenuations on the control section are essentially unity for $k = 60{,}000$ lb/in. Presented in figure 8(b) are the responses on the bottom center of the epoxy bonded panels. Appreciable but somewhat less effectiveness was obtained through the use of the isolation mounts for responses at this location on the model.

Although the results indicate that reductions in the structural amplifications can be obtained by utilizing isolation mounts, several disadvantages are also presented. One such undesirable feature is that large lateral movements because of rocking action of the panels, control section, and struts on the isolators can occur at the isolator natural frequency. This presents the additional complication of possible interference of the model or vehicle panels with the launch-vehicle shroud. Further, for omnidirectional isolators to provide desired isolation large deflections are often necessary. The deflections are needed to prevent bottoming out of the isolators under the loading imposed by the increasing acceleration of the launch vehicle during the flight. Sacrifice of onmidirectional isolation for unidirectional isolation could possibly overcome some of the disadvantages.

Effects of stiffness between control and sensory sections.- To assess the effects of stiffness between the control and the sensory section on the response of the model, structural amplifications as a function of frequency were determined for values of k equal to 60,000 lb/in. and 15,250 lb/in. Typical results of this study are presented in figure 9 which shows the measured model response to inputs along the pitch axis for the bottom center of the solar panel. The results

indicate that increased stiffness between the two sections leads to only slight increases in panel amplifications at somewhat increased frequencies.

Sensory section response.- As might be intuitively expected, little, if any, reductions in the measured response in the compartments of the sensory section were noted when changes were made in the structure above the sensory section. As an illustration of the responses that occurred around the sensory section, peak values of the amplifications in several compartments were measured and are presented in figure 10. Maximum structural amplifications were found to occur at or near the compartment panel natural frequencies with the overall amplification magnitude being less severe than these maximums.

CONCLUDING REMARKS

An investigation has been conducted to evaluate the effectiveness of damping and isolation methods in reducing the structural amplifications of vibratory inputs on a simplified scale model of the Nimbus spacecraft. The results are summarized in the following paragraphs.

1. Experimental frequencies for the first 10 modes of the solar panels on the 1/2-scale model were compared with calculated values using a finite-difference method. In general, good agreement between the calculated and experimental frequencies was found. Fair agreement was also shown between the computed and experimental node locations.

2. A comparison of the model response to full-scale vehicle response at the base of the control section for inputs along the pitch axis indicated that general agreement existed between model and full-scale vehicle resonances in the frequency range up to approximately 35 cps.

3. In the evaluation of the effects of distributed damping in the solar panels the results emphasized (a) that very high amplifications exist in such structures, (b) that the many structural resonances were associated mainly with the natural modes of the panels, and (c) that the response of such a structure to unsteady forces can be substantially reduced, in most instances, by the use of damping materials at suitably chosen points.

4. Isolation mounts were more effective in reducing the magnitude of structural amplifications on the epoxy bonded, lightly damped, solar panels than the inherently damped panels. The combination of both isolation mounts and damped panels was extremely effective in reducing the magnitude of detectable structural resonances.

5. Increased stiffness between the control section and the sensory section resulted in only slight increases in panel amplifications at somewhat increased frequencies.

6. Little, if any, reductions in the measured response in the compartments around the sensory section were noted when changes were made in the structure above the sensory section.

APPENDIX

PLANFORMS AND COMPUTING MACHINE INPUTS FOR CALCULATING MODES AND FREQUENCIES OF THE SOLAR PANEL

This appendix is included to present information required in conjunction with the procedure given in reference 1 for calculating the modes and frequencies of the simulated solar panels. Figure 11 presents the planform of the solar panel for the case of hinged-hinged edge conditions assumed along the length of the panel. Included in table 1 are the computing machine inputs necessary for calculating the modes and frequencies of the panel with these assumed edge conditions.

Symbols included in figure 11 and table 1 are:

D	panel flexural rigidity, $E\left[\frac{(2h + t)^3 - t^3}{12}\right]$, in-lb
E	Young's modulus of elasticity, $lb/in.^2$
h	panel skin thickness, in.
K	number of moving mass points on the solar panel planform
L	length of solar panel, in.
m	mass per unit area of panel, $lb\text{-}sec^2/in.^3$
R	number of unknown deflections left in the expression for energy after conditions of constraint have been applied
T	total number of points on the solar panel planform
t	core thickness of panel section, in.
ϵ	horizontal distance between vertical grid lines on panel planform
λ	vertical distance between horizontal grid lines on panel planform
μ	Poisson's ratio

Subscript:

r denotes any convenient reference of a quantity

Computing machine outputs of particular interest include deflections in the natural mode shapes at the mass stations which move, and the dimensionless eigenvalues, Ω, which are related to the natural frequencies of the plate by the formula

$$f_c = \frac{1}{2\pi\epsilon^2}\sqrt{\frac{D_r\Omega}{2m_r}}, \text{ cps}$$

REFERENCES

1. Walton, William C., Jr.: Applications of a General Finite-Difference Method for Calculating Bending Deformations of Solid Plates. NASA TN D-536, 1960.

2. Harris, Cyril M., and Crede, Charles E., eds.: Shock and Vibration Handbook. Vol. 2, McGraw-Hill Book Company, Inc. (New York), c.1961. Section 32, pp. 40-41, Section 36-37.

TABLE 1.- COMPUTING-MACHINE INPUT FOR CALCULATION OF MODES AND FREQUENCIES OF SOLAR PANEL

FOR HINGED-HINGED EDGES ALONG PANEL LENGTH

[L = 48 in.; ϵ/λ = 1.136; μ = 0.333; K = 44; R = 78; T = 100; D_r = 428 in-lb; m_r = 0.00083 lb-sec^2/in.^{3} (see ref. 1)]

(1)	(2)	(3)	(4)	(5)	(6)	(7)	(8)	(9)	(10)	(11)	(12)	(13)	(14)	(15)	(16)	(17)
Gridpoint number	$\bar{D}_0\alpha_0$	$\bar{D}_{NE/2}\alpha_{NE/2}$	N_{NN}	N_{NW}	N_N	N_{NE}	N_{WW}	N_W	N_0	N_E	N_{EE}	N_{SW}	N_S	N_{SE}	N_{SS}	$\bar{m}_0\alpha_0$
1	0.297	0.297	51	50	79	80	0	49	1	2	3	48	12	13	23	1
2	.474	.474	52	79	80	81	49	1	2	3	4	12	13	14	24	1
3	.650	.650	53	80	81	82	1	2	3	4	5	13	14	15	25	1
4	.827	.827	54	81	82	83	2	3	4	5	6	14	15	16	26	1
5	1	1	55	82	83	84	3	4	5	6	7	15	16	17	27	1
6	1	1	56	83	84	85	4	5	6	7	8	16	17	18	28	1
7	1	.827	57	84	85	86	5	6	7	8	9	17	18	19	29	1
8	.827	.650	58	85	86	87	6	7	8	9	10	18	19	20	30	1
9	.650	.474	59	86	87	88	7	8	9	10	11	19	20	21	31	1
10	.474	.297	60	87	88	89	8	9	10	11	63	20	21	22	32	1
11	.297	.1485	61	88	89	62	9	10	11	63	0	21	22	64	33	1
12	.297	.297	79	49	1	2	0	48	12	13	14	47	23	24	34	1
13	.474	.474	80	1	2	3	48	12	13	14	15	23	24	25	35	1
14	.650	.650	81	2	3	4	12	13	14	15	16	24	25	26	36	1
15	.827	.827	82	3	4	5	13	14	15	16	17	25	26	27	37	1
16	1	1	83	4	5	6	14	15	16	17	18	26	27	28	38	1
17	1	1	84	5	6	7	15	16	17	18	19	27	28	29	39	1
18	1	.827	85	6	7	8	16	17	18	19	20	28	29	30	40	1
19	.827	.650	86	7	8	9	17	18	19	20	21	29	30	31	41	1
20	.650	.474	87	8	9	10	18	19	20	21	22	30	31	32	42	1
21	.474	.297	88	9	10	11	19	20	21	22	64	31	32	33	43	1
22	.297	.1485	89	10	11	63	20	21	22	64	0	32	33	65	44	1
23	.297	.297	1	48	12	13	0	47	23	24	25	46	34	35	90	1
24	.474	.474	2	12	13	14	47	23	24	25	26	34	35	36	91	1
25	.650	.650	3	13	14	15	23	24	25	26	27	35	36	37	92	1
26	.827	.827	4	14	15	16	24	25	26	27	28	36	37	38	93	1
27	1	1	5	15	16	17	25	26	27	28	29	37	38	39	94	1
28	1	1	6	16	17	18	26	27	28	29	30	38	39	40	95	1
29	1	.827	7	17	18	19	27	28	29	30	31	39	40	41	96	1
30	.827	.650	8	18	19	20	28	29	30	31	32	40	41	42	97	1
31	.650	.474	9	19	20	21	29	30	31	32	33	41	42	43	98	1
32	.474	.297	10	20	21	22	30	31	32	33	65	42	43	44	99	1
33	.297	.1485	11	21	22	64	31	32	33	65	0	43	44	66	100	1
34	.297	.297	12	47	23	24	0	46	34	35	36	45	90	91	78	1
35	.474	.474	13	23	24	25	46	34	35	36	37	90	91	92	77	1
36	.650	.650	14	24	25	26	34	35	36	37	38	91	92	93	76	1
37	.827	.827	15	25	26	27	35	36	37	38	39	92	93	94	75	1
38	1	1	16	26	27	28	36	37	38	39	40	93	94	95	74	1
39	1	1	17	27	28	29	37	38	39	40	41	94	95	96	73	1
40	1	.827	18	28	29	30	38	39	40	41	42	95	96	97	72	1
41	.827	.650	19	29	30	31	39	40	41	42	43	96	97	98	71	1
42	.650	.474	20	30	31	32	40	41	42	43	44	97	98	99	70	1
43	.474	.297	21	31	32	33	41	42	43	44	66	98	99	100	69	1
44	.297	.1485	22	32	33	65	42	43	44	66	0	99	100	67	68	1
45	0	.1485	47	0	46	34	0	0	45	90	91	0	0	78	0	
46	0	.1485	48	0	47	23	0	0	46	34	35	0	45	90	0	
47	0	.1485	49	0	48	12	0	0	47	23	24	0	46	34	45	
48	0	.1485	50	0	49	1	0	0	48	12	13	0	47	23	46	
49	0	.1485	0	0	50	79	0	0	49	1	2	0	48	12	47	
50	0	0	0	0	0	51	0	0	50	79	80	0	49	1	48	

(1)	(2)	(3)	(4)	(5)	(6)	(7)	(8)	(9)	(10)	(11)	(12)	(13)	(14)	(15)	(16)	(17)
Gridpoint number	$\bar{D}_0\alpha_0$	$\bar{D}_{NE/2}\alpha_{NE/2}$	N_{NN}	N_{NW}	N_N	N_{NE}	N_{WW}	N_W	N_0	N_E	N_{EE}	N_{SW}	N_S	N_{SE}	N_{SS}	$\bar{m}_0\alpha_0$
51	0	0	0	0	0	0	0	0	51	52	53	50	79	80	1	
52	0	0	0	0	0	0	0	51	52	53	54	79	80	81	2	
53	0	0	0	0	0	0	51	52	53	54	55	80	81	82	3	
54	0	0	0	0	0	0	52	53	54	55	56	81	82	83	4	
55	0	0	0	0	0	0	53	54	55	56	57	82	83	84	5	
56	0	0	0	0	0	0	54	55	56	57	58	83	84	85	6	
57	0	0	0	0	0	0	55	56	57	58	59	84	85	86	7	
58	0	0	0	0	0	0	56	57	58	59	60	85	86	87	8	
59	0	0	0	0	0	0	57	58	59	60	61	86	87	88	9	
60	0	0	0	0	0	0	58	59	60	61	0	87	88	89	10	
61	0	0	0	0	0	0	59	60	61	0	0	88	89	62	11	
62	0	0	0	61	0	0	88	89	62	0	0	11	63	0	64	
63	0	0	0	89	62	0	10	11	63	0	0	22	64	0	65	
64	0	0	62	11	63	0	21	22	64	0	0	33	65	0	66	
65	0	0	63	22	64	0	32	33	65	0	0	44	66	0	67	
66	0	0	64	33	65	0	43	44	66	0	0	100	67	0	0	
67	0	0	65	44	66	0	99	100	67	0	0	68	0	0	0	
68	0	0	44	99	100	67	70	69	68	0	0	0	0	0	0	
69	0	0	43	98	99	100	71	70	69	68	0	0	0	0	0	
70	0	0	42	97	98	99	72	71	70	69	68	0	0	0	0	
71	0	0	41	96	97	98	73	72	71	70	69	0	0	0	0	
72	0	0	40	95	96	97	74	73	72	71	70	0	0	0	0	
73	0	0	39	94	95	96	75	74	73	72	71	0	0	0	0	
74	0	0	38	93	94	95	76	75	74	73	72	0	0	0	0	
75	0	0	37	92	93	94	77	76	75	74	73	0	0	0	0	
76	0	0	36	91	92	93	78	77	76	75	74	0	0	0	0	
77	0	0	35	90	91	92	0	78	77	76	75	0	0	0	0	
78	0	0	34	45	90	91	0	0	78	77	76	0	0	0	0	
79	.1485	0														
80	.237	0														
81	.325	0														
82	.4135	0														
83	.5	0														
84	.5	0														
85	.5	0														
86	.4135	0														
87	.325	0														
88	.237	0														
89	.1485	0														
90	.1485	.297														
91	.237	.474														
92	.325	.650														
93	.4135	.827														
94	.5	1														
95	.5	1														
96	.5	.827														
97	.4135	.650														
98	.325	.474														
99	.237	.297														
100	.1485	.1485														

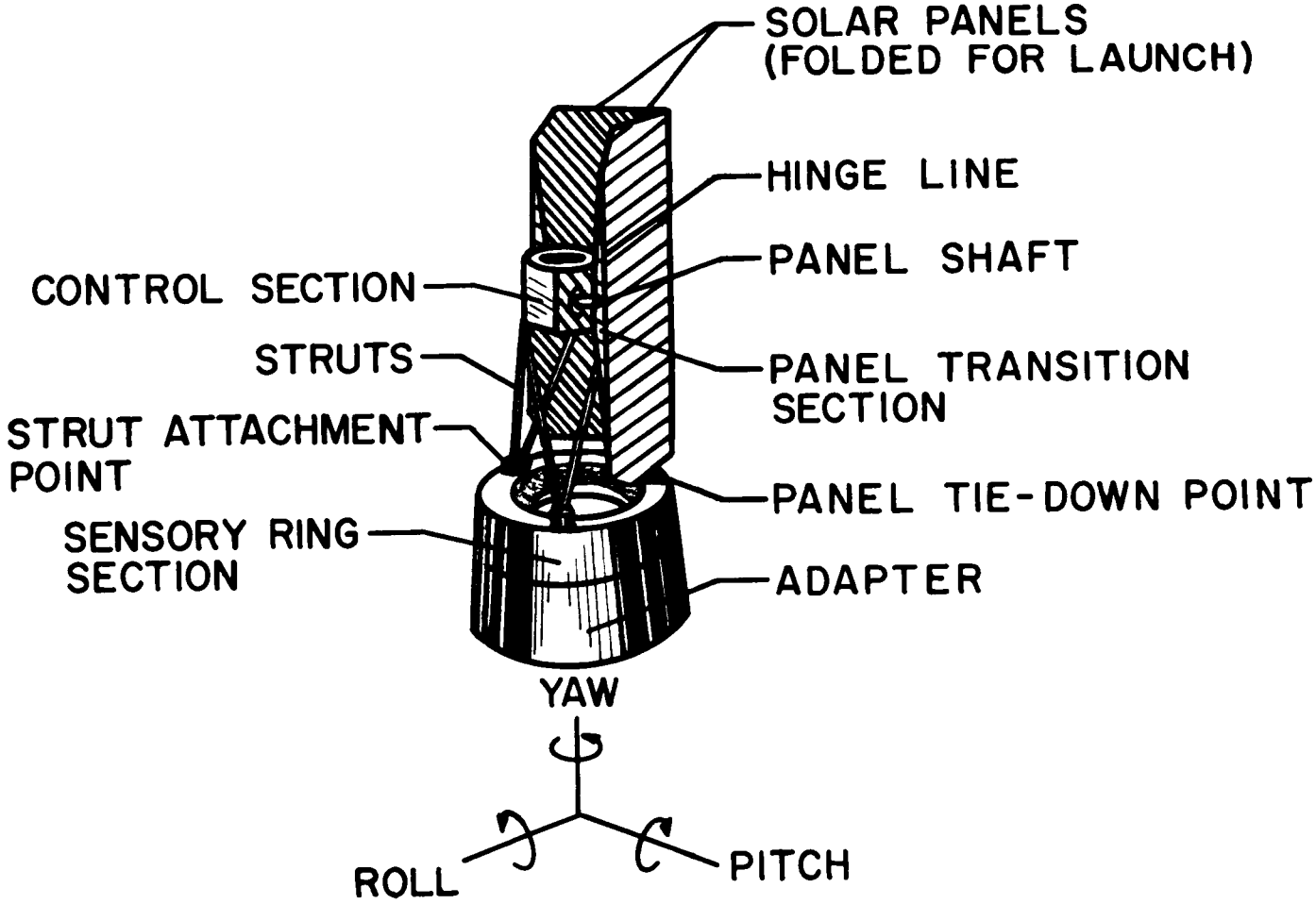

NASA

Figure 1.- General configuration and elements of the 1/2-scale Nimbus model.

PRINCIPAL DIMENSIONS	INCHES
CONTROL BOX WIDTH	A- 11
SOLOR PANEL WIDTH	B- 19.2
SOLOR PANEL LENGTH	C- 48
LENGTH, OVERALL (ADAPTER INCLUDED)	D- 69
SENSORY RING HEIGHT	E- 6.5
SPACECRAFT ADAPTER HEIGHT	F- 12
SENSORY RING DIAMETER	G- 27.5
SPACECRAFT ADAPTER DIAMETER (BOTTOM DIAMETER)	H- 30

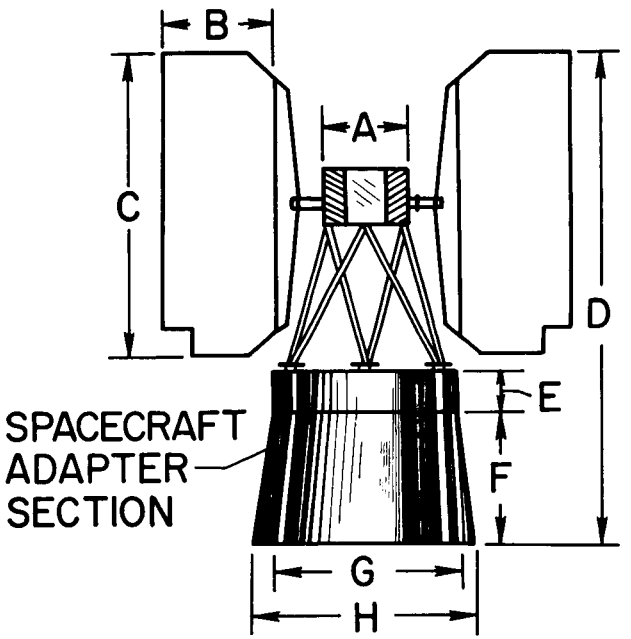

NASA

Figure 2.- Principal dimensions of the 1/2-scale Nimbus model.

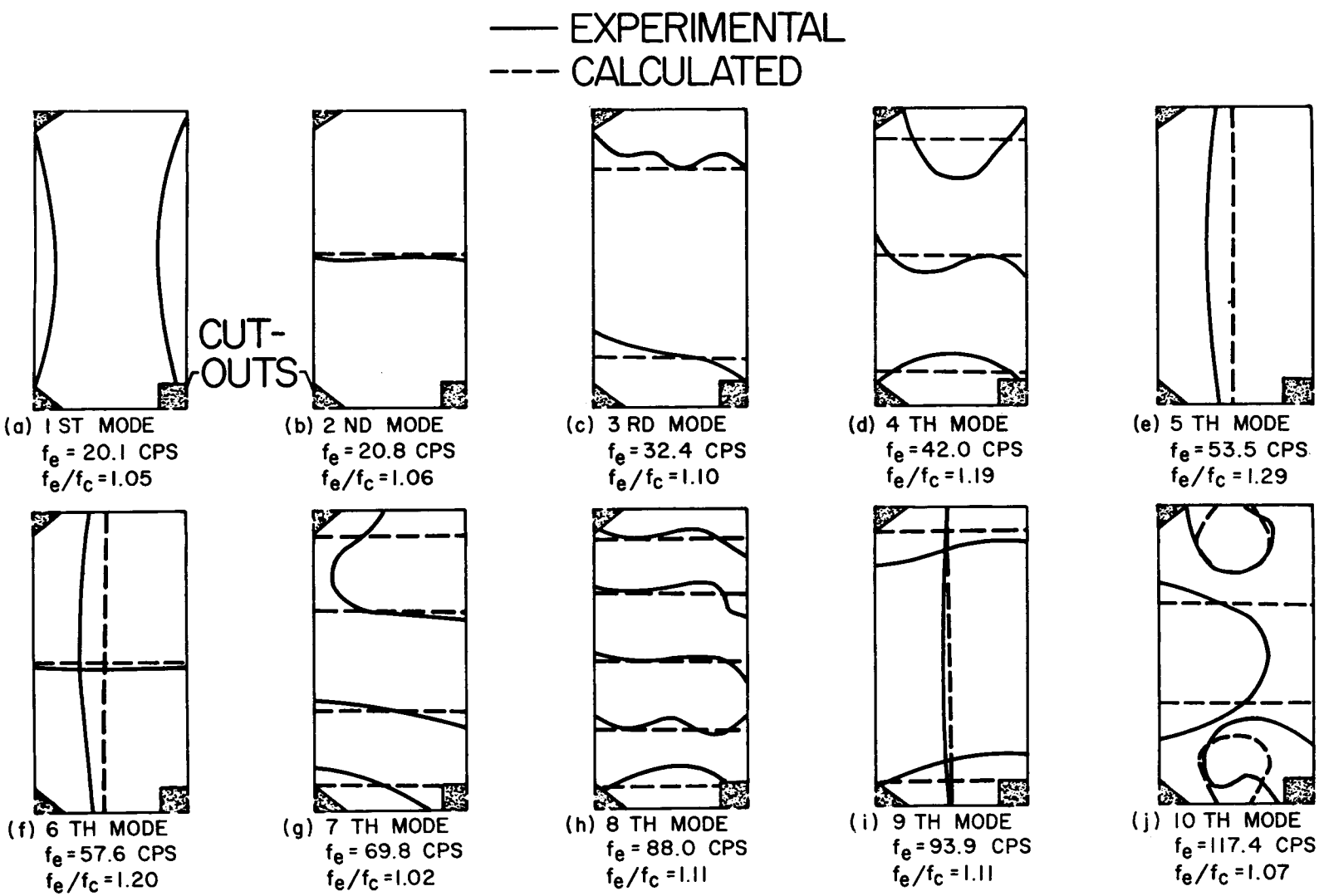

Figure 3.- Comparison of experimental and calculated modes and frequencies of the simulated solar panel.

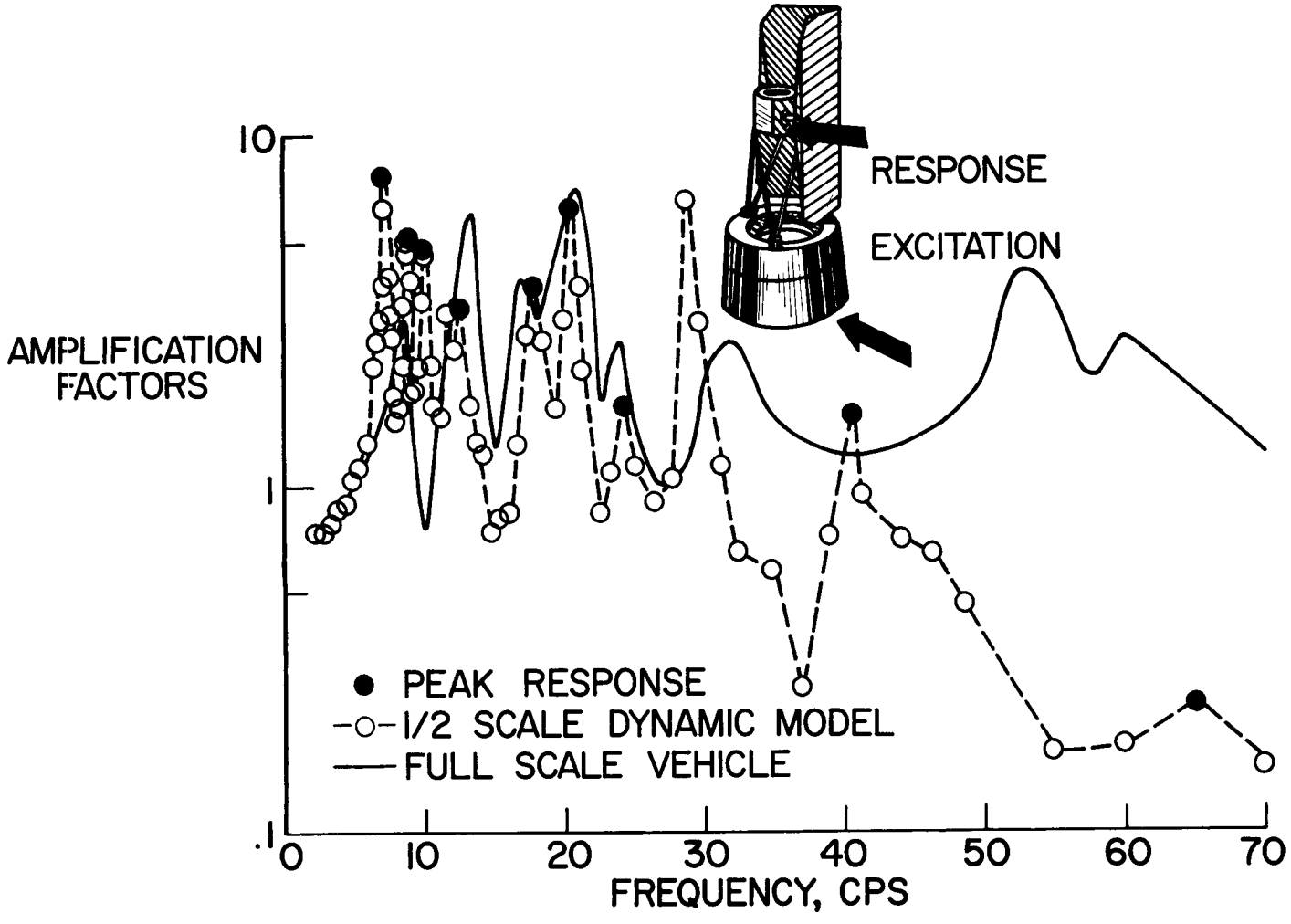

Figure 4.- Comparison of responses at the base of control section on 1/2-scale model and full-scale spacecraft. Excitation along pitch axis. Model frequencies divided by 2.

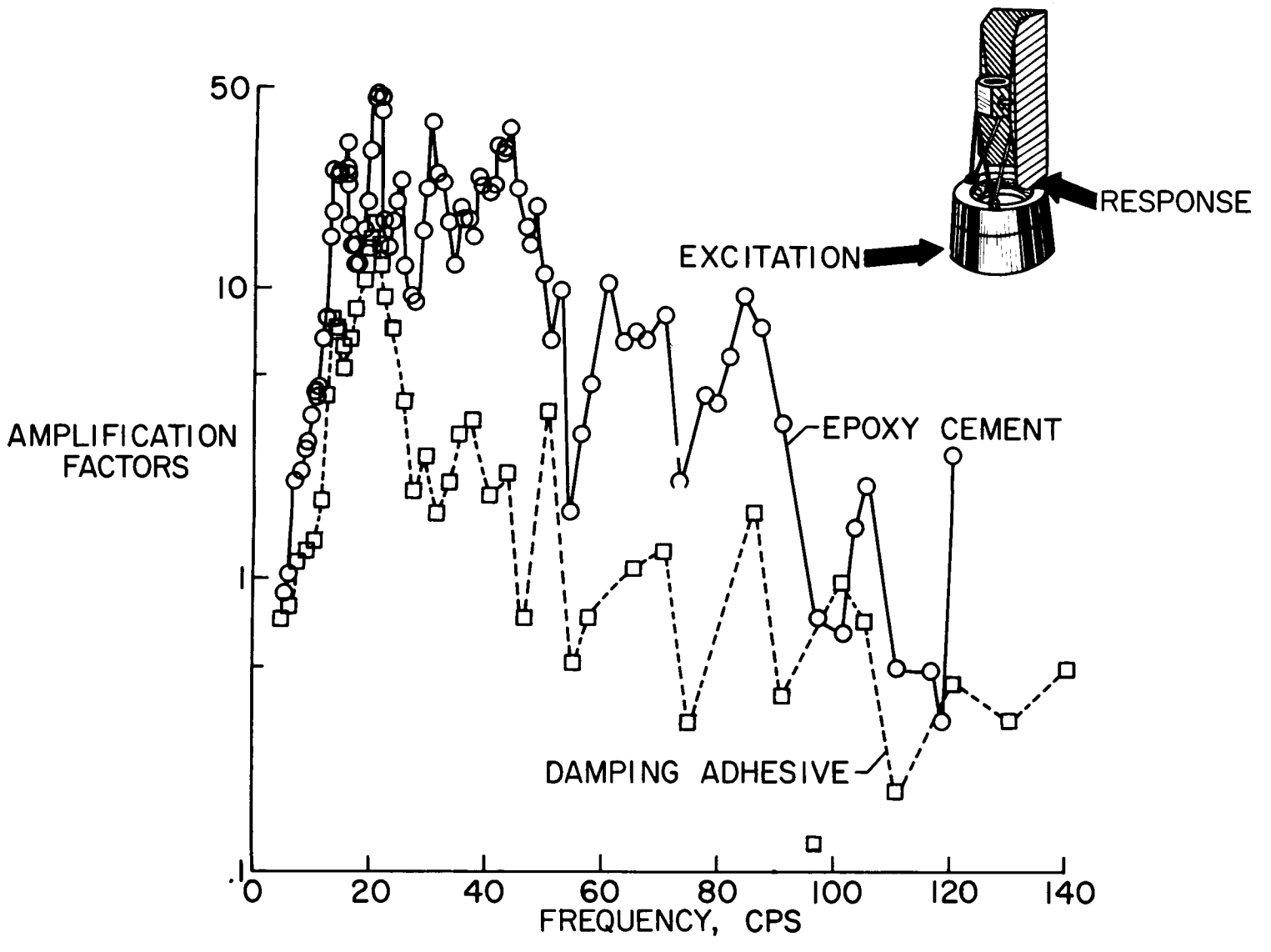

(a) Response at bottom center of solar panel. NASA

Figure 5.- Dynamic amplification as a function of excitation frequency. k = 15,250 lb/in. Excitation along roll axis.

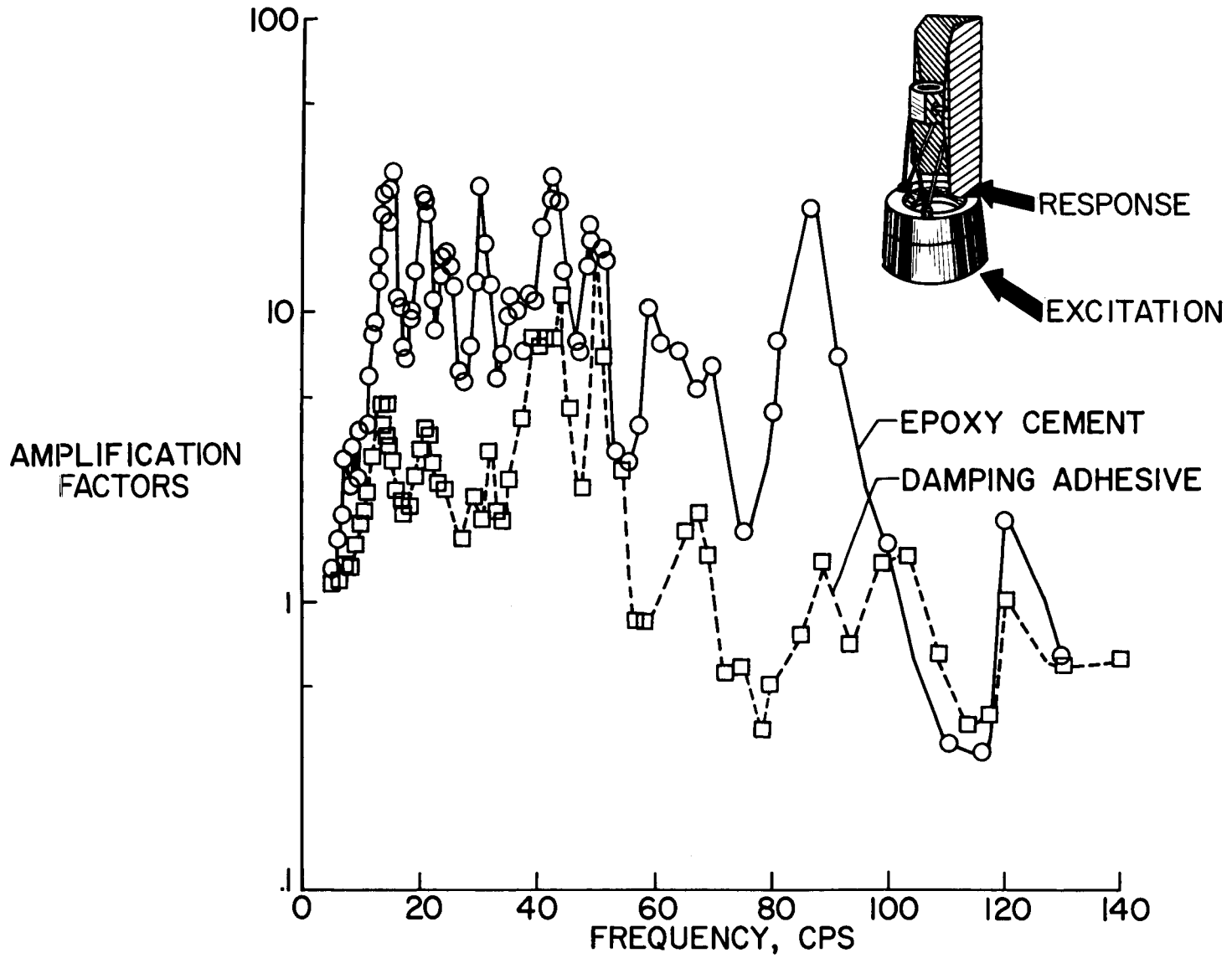

(b) Response at bottom of hinge line on panel transition. NASA

Figure 5.- Continued.

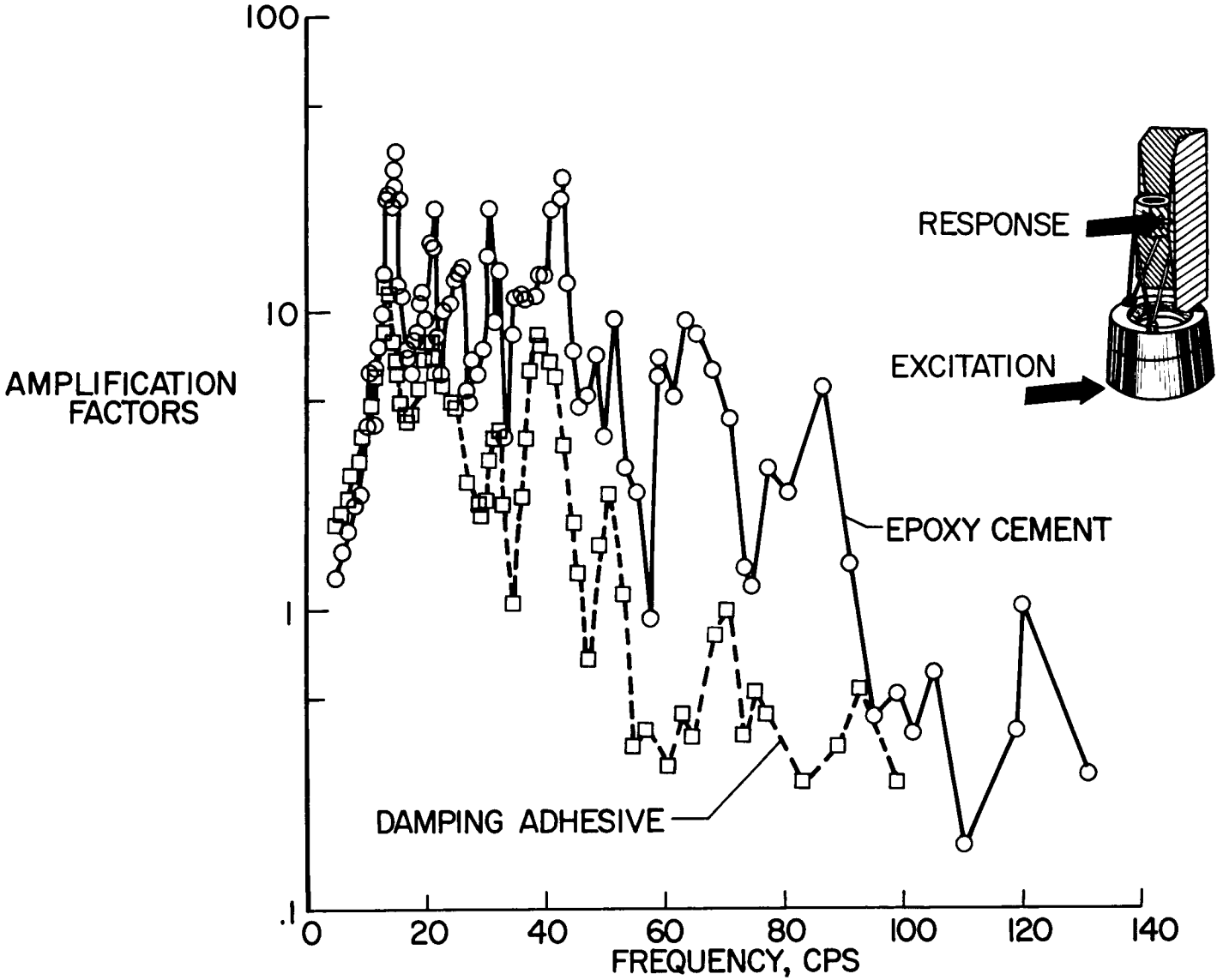

(c) Response at end of panel shaft.

NASA

Figure 5.- Continued.

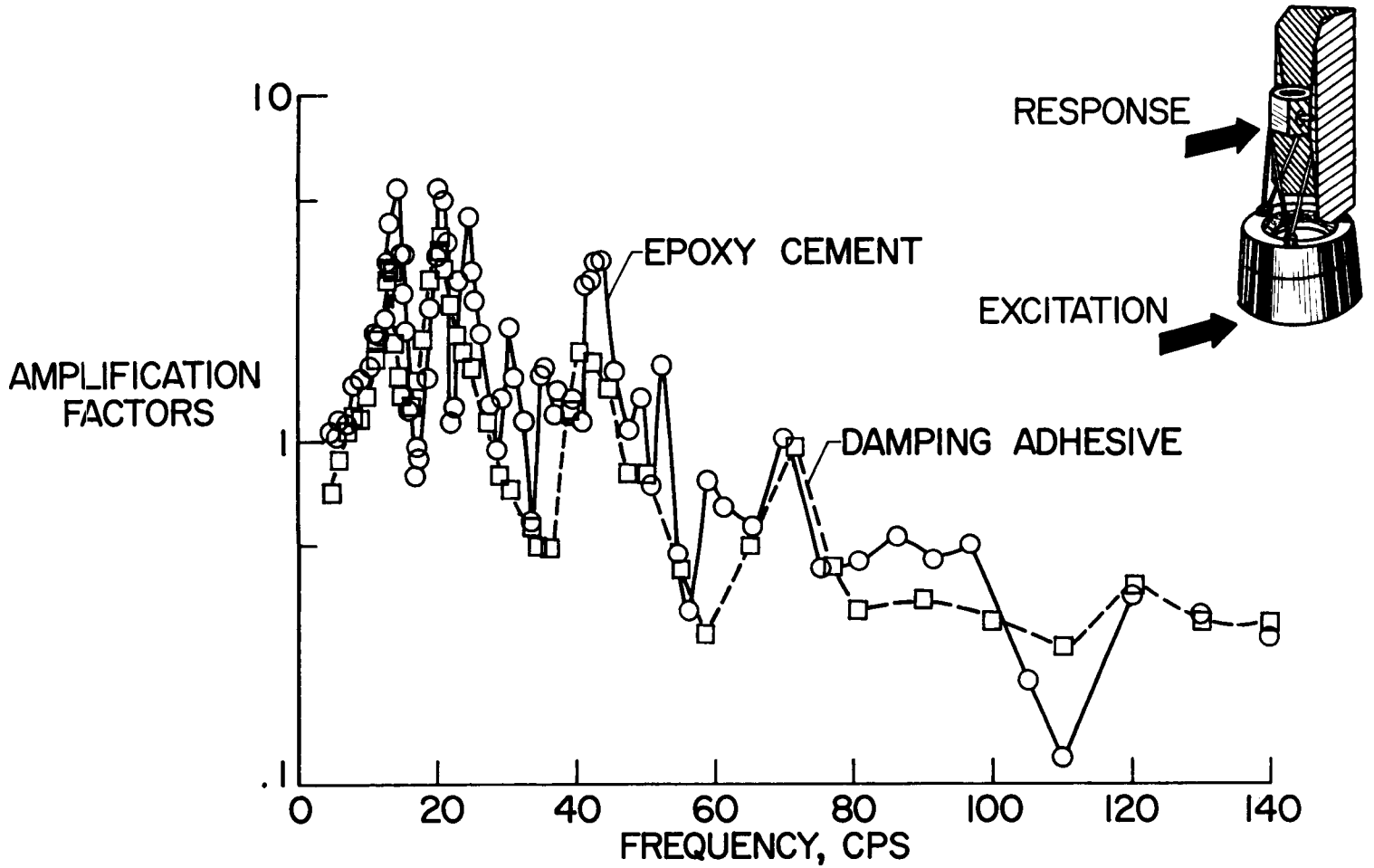

(d) Response at base of control section. NASA

Figure 5.- Concluded.

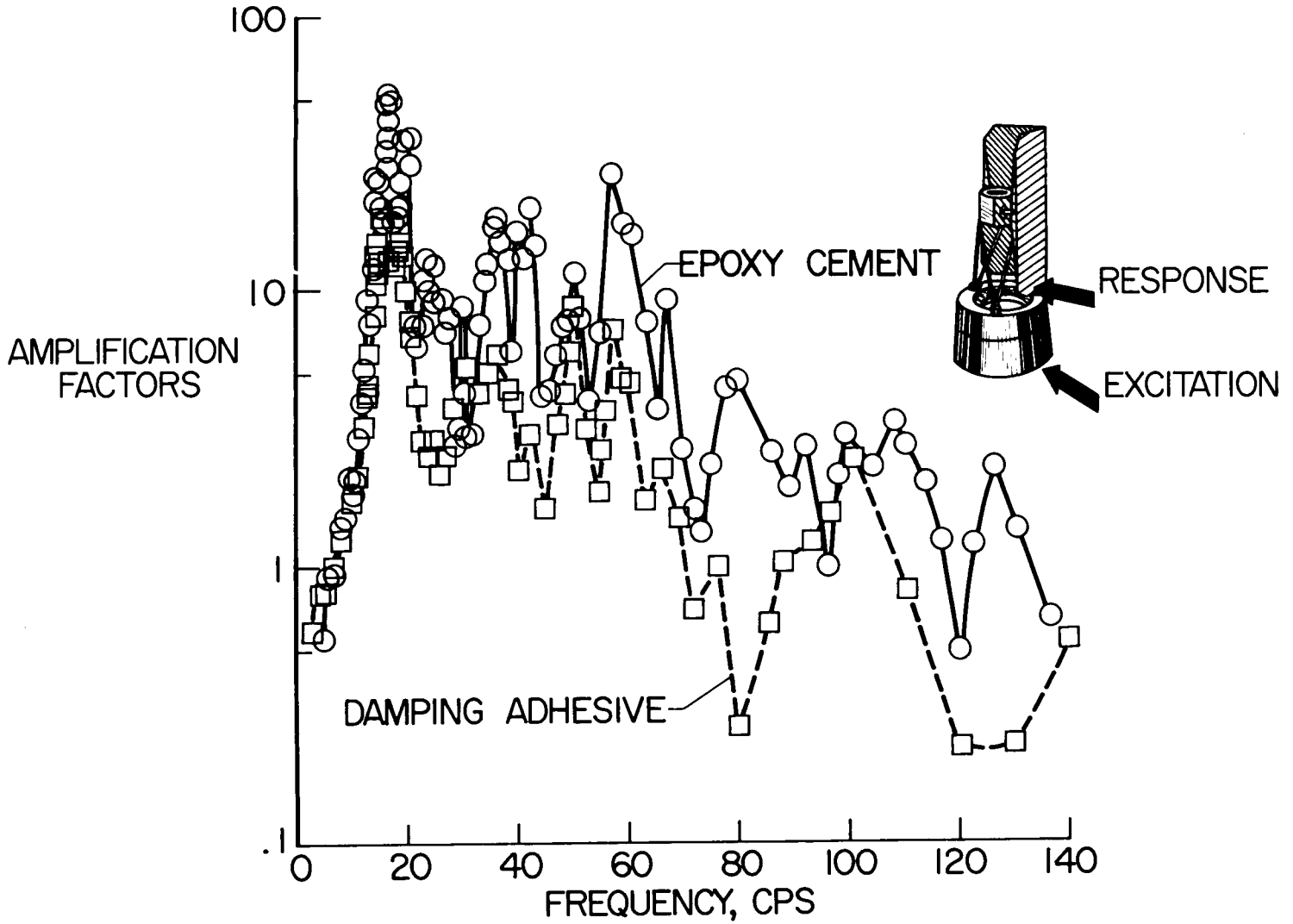

(a) Response at bottom center of solar panel.

NASA

Figure 6.- Dynamic amplification as a function of excitation frequency. k = 15,250 lb/in. Excitation along pitch axis.

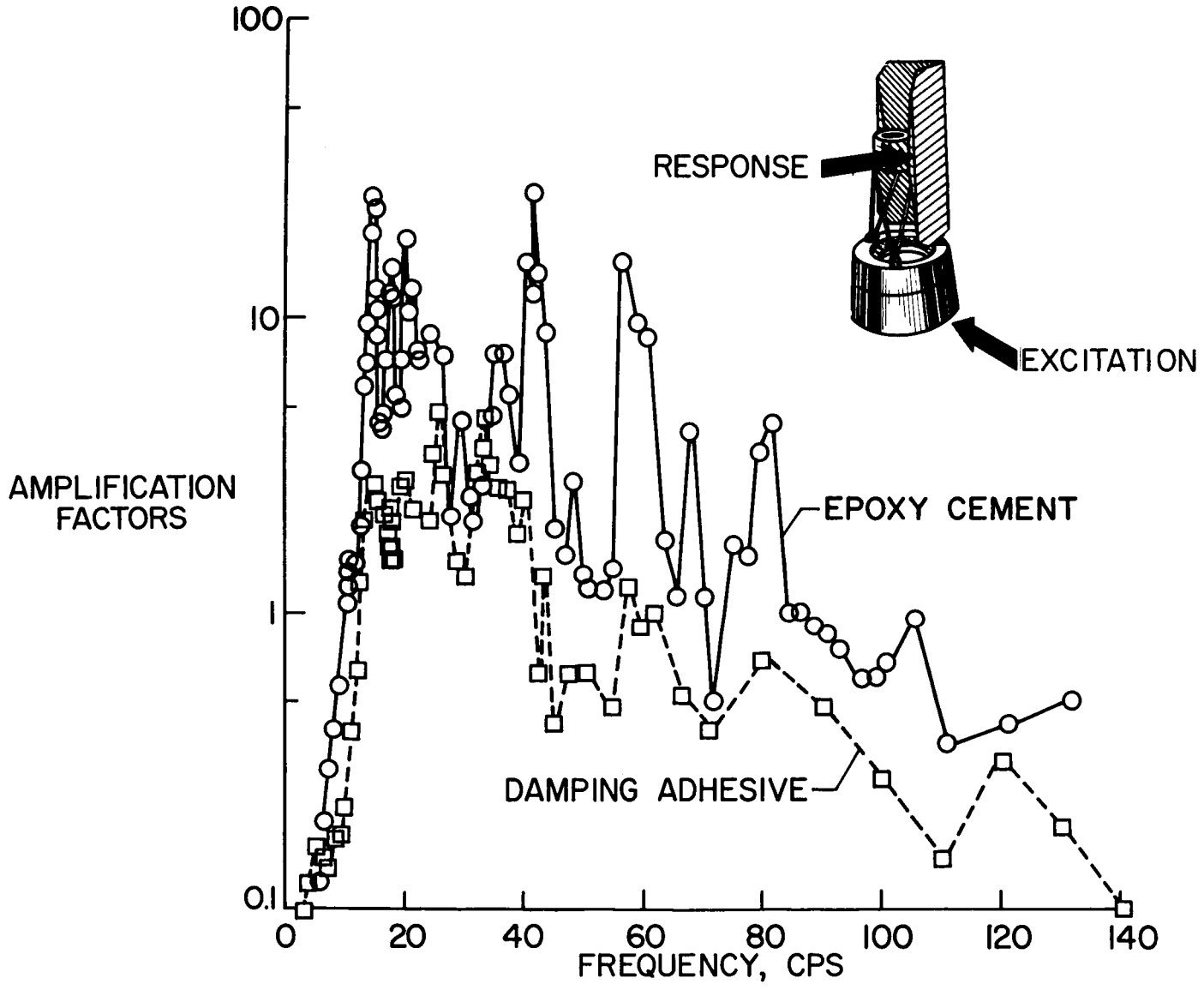

(b) Response at end of panel shaft. NASA

Figure 6.- Continued.

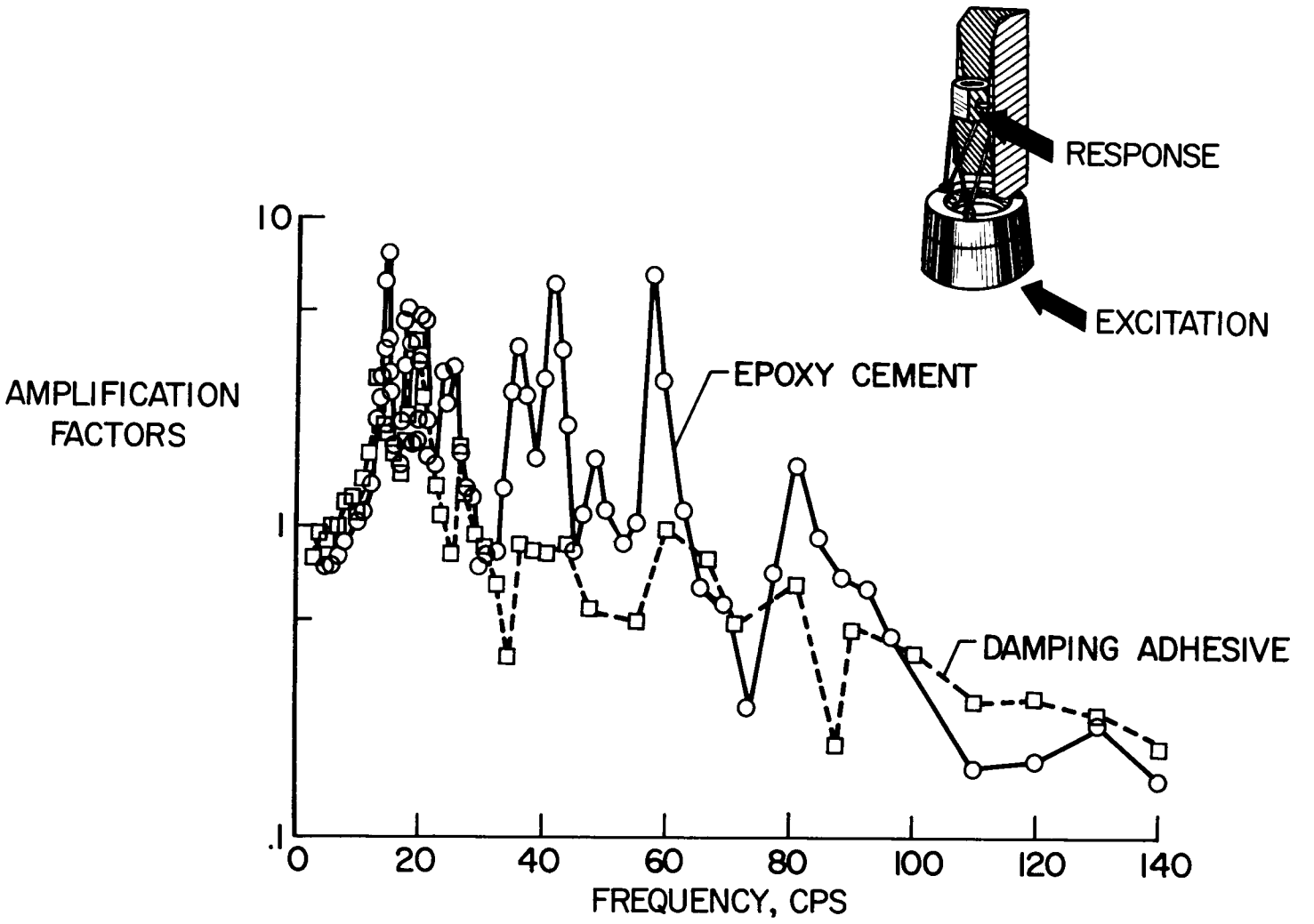

(c) Response at base of control section.

NASA

Figure 6.- Concluded.

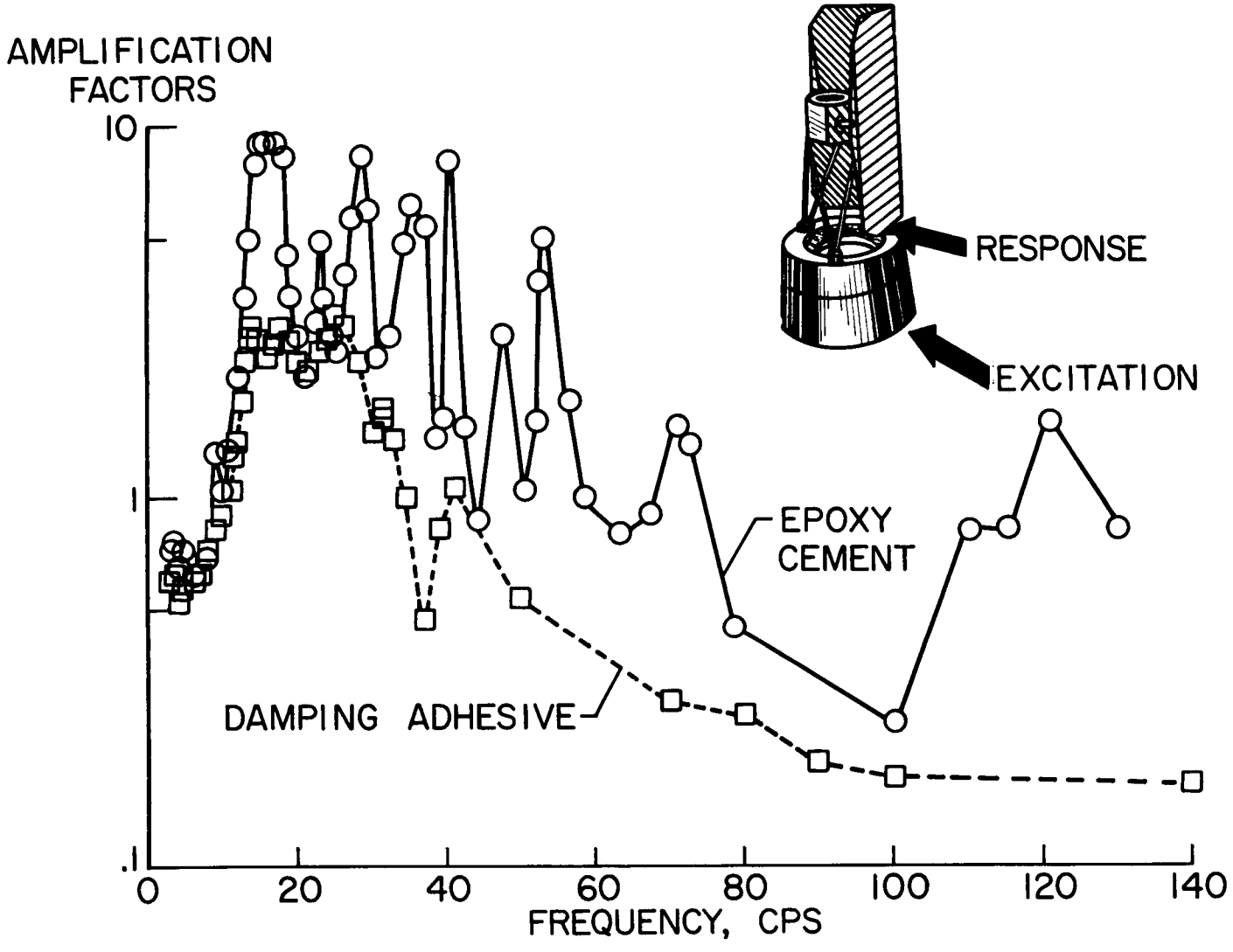

NASA

Figure 7.- Dynamic amplification as a function of excitation frequency.

Isolators $\begin{cases} 2{:}5\frac{1}{2} - 12\frac{1}{2} \text{ lb} \\ 1{:}20 \text{ lb} \end{cases}$. Excitation along pitch axis.

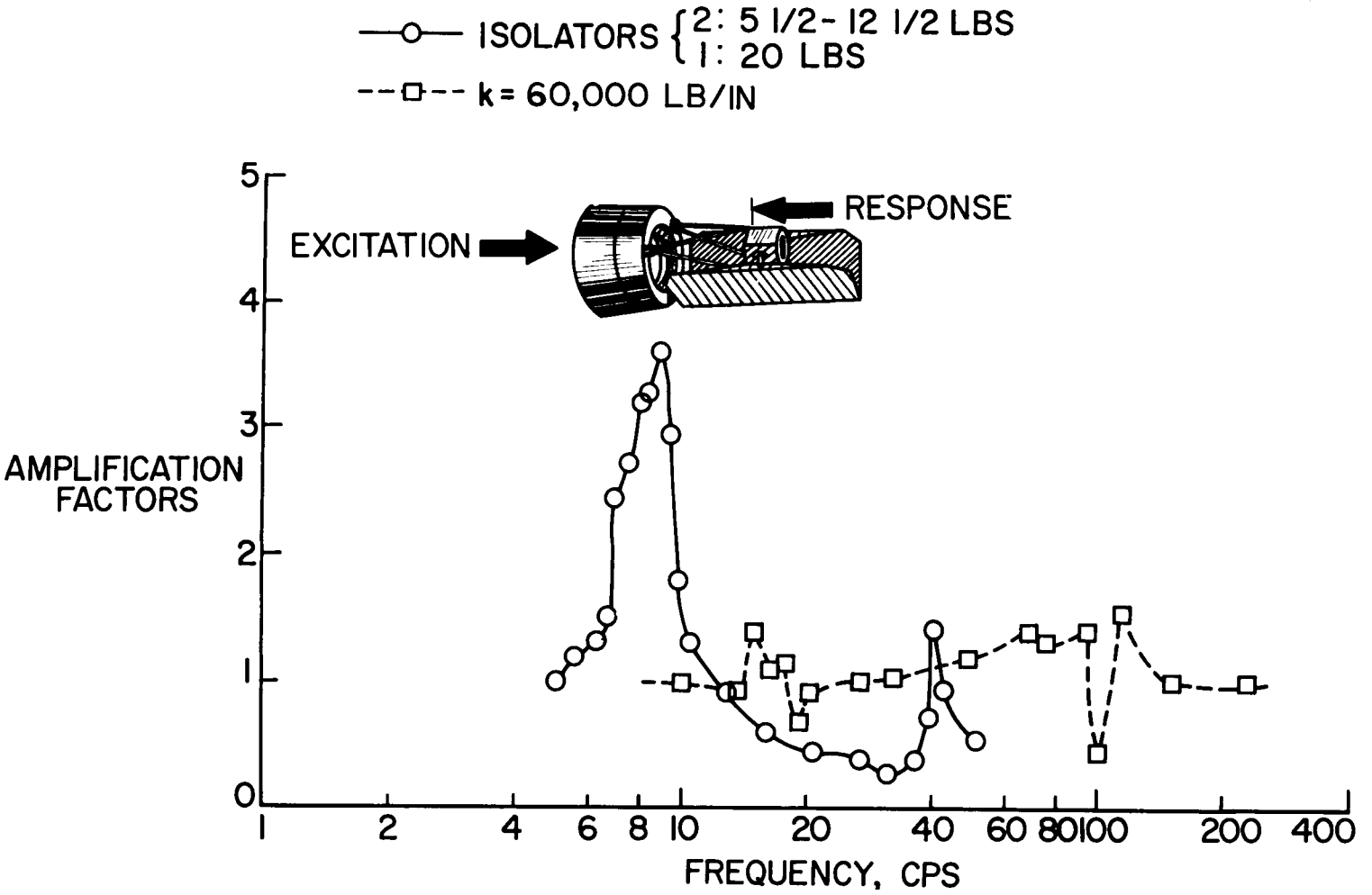

(a) Response at base of control section.

NASA

Figure 8.- Dynamic amplification as a function of excitation frequency. Excitation along yaw axis.

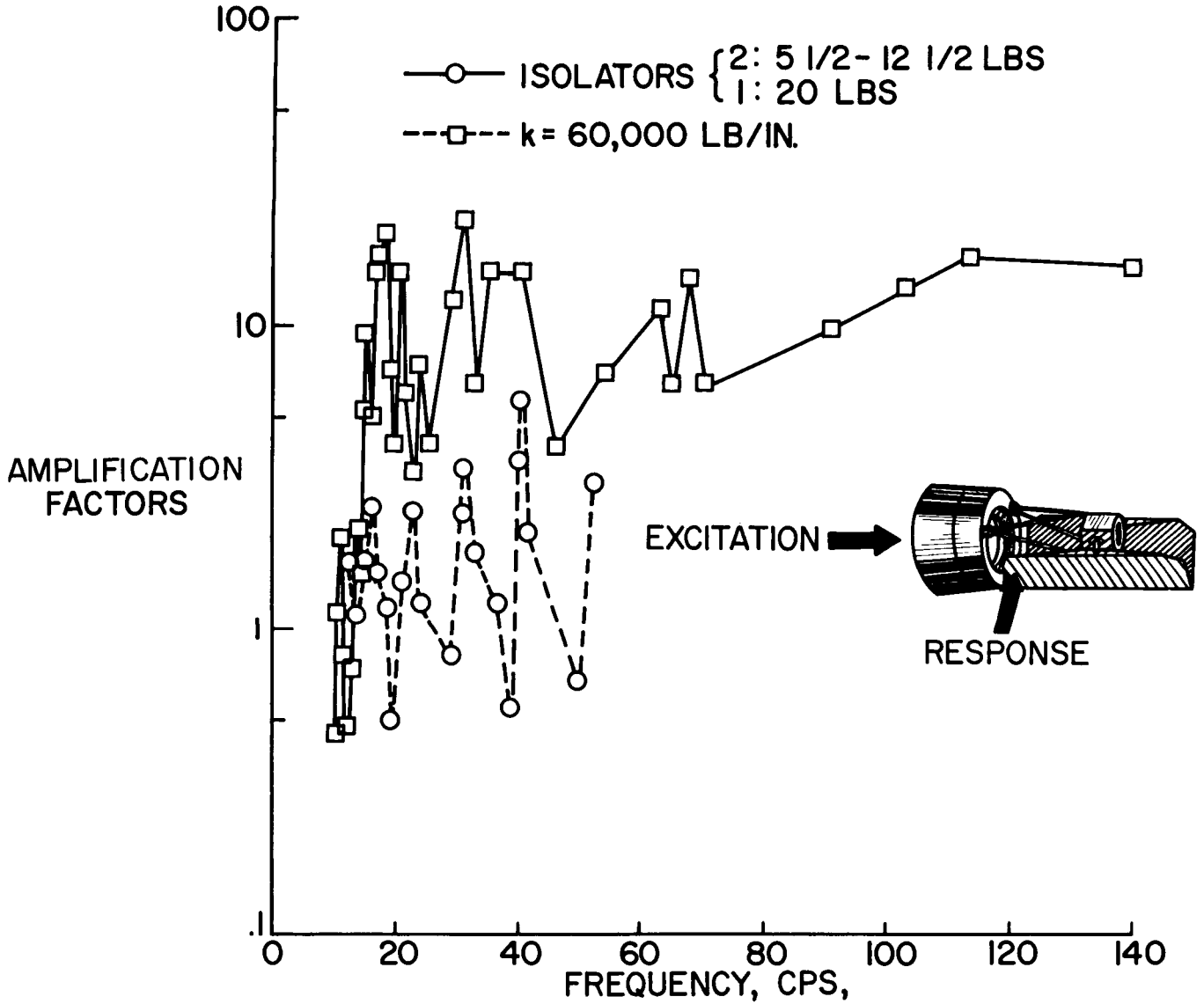

(b) Response at bottom center of solar panel. NASA

Figure 8.- Concluded.

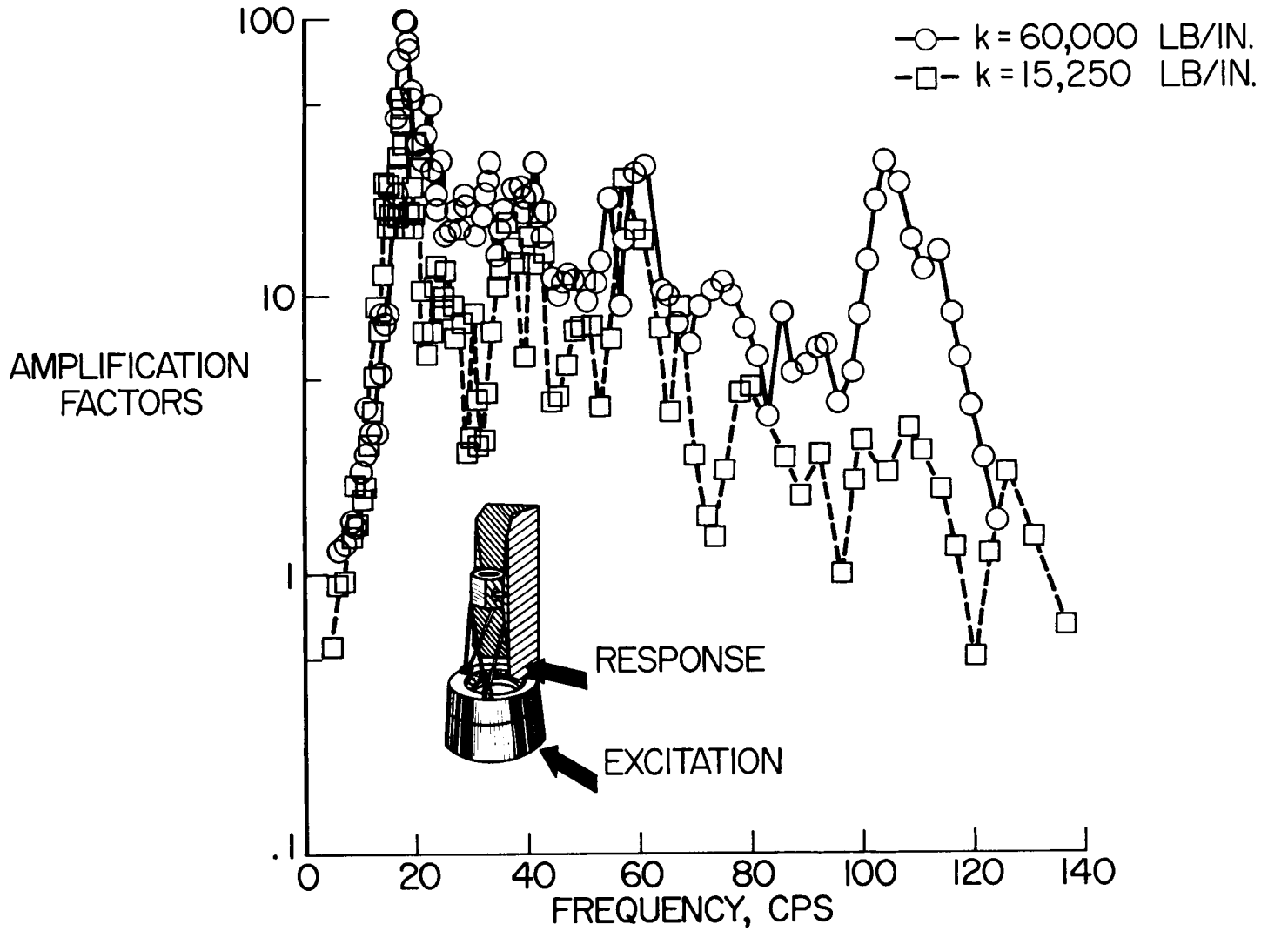

NASA

Figure 9.- Effects of stiffness between control and sensory sections on dynamic amplification. Response at bottom center of epoxy-bonded solar panel. Excitation along pitch axis.

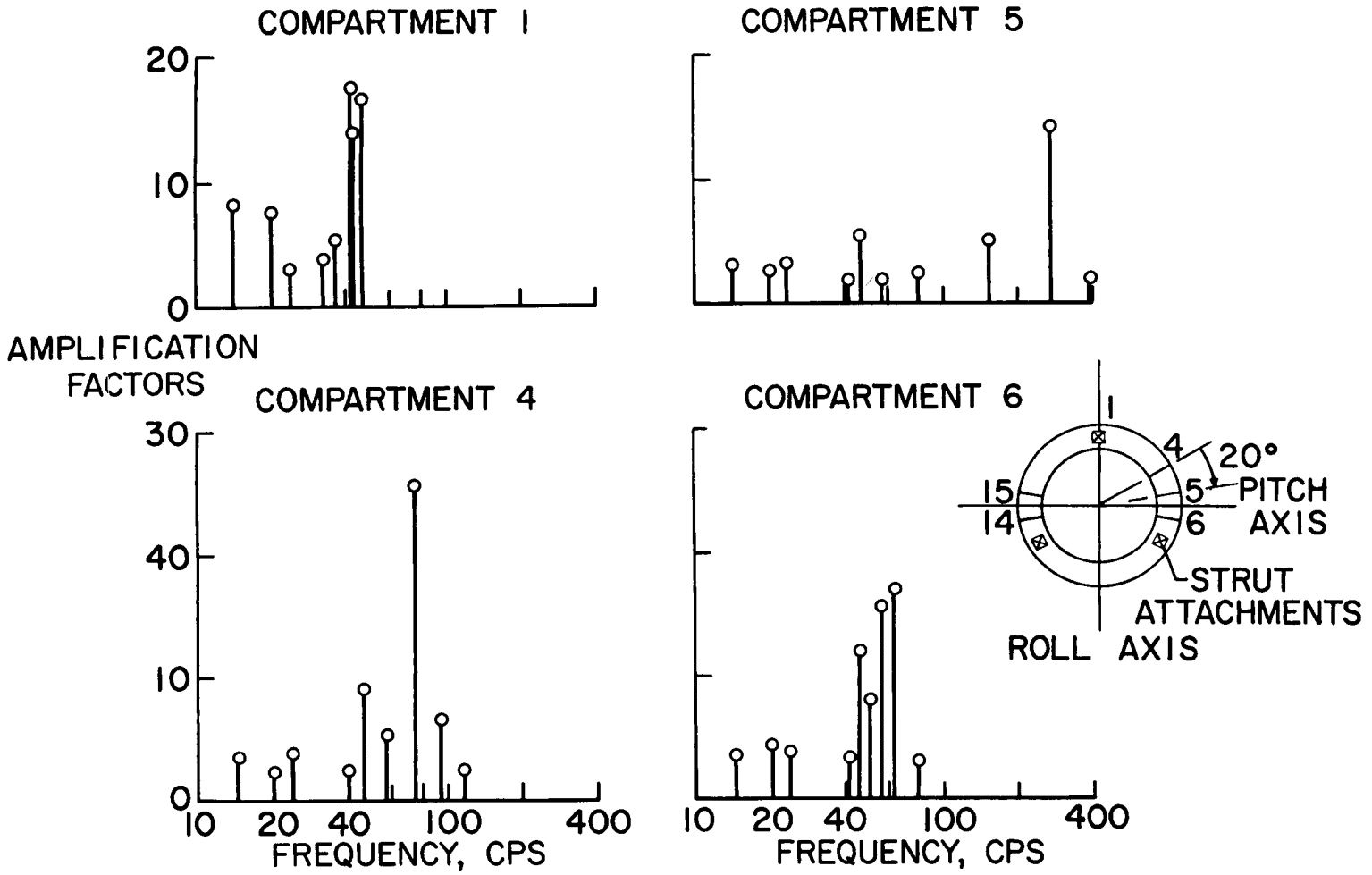

NASA

Figure 10.- Peak values of dynamic amplification as a function of excitation frequency. Response in sensory section compartments. Excitation along roll axis.

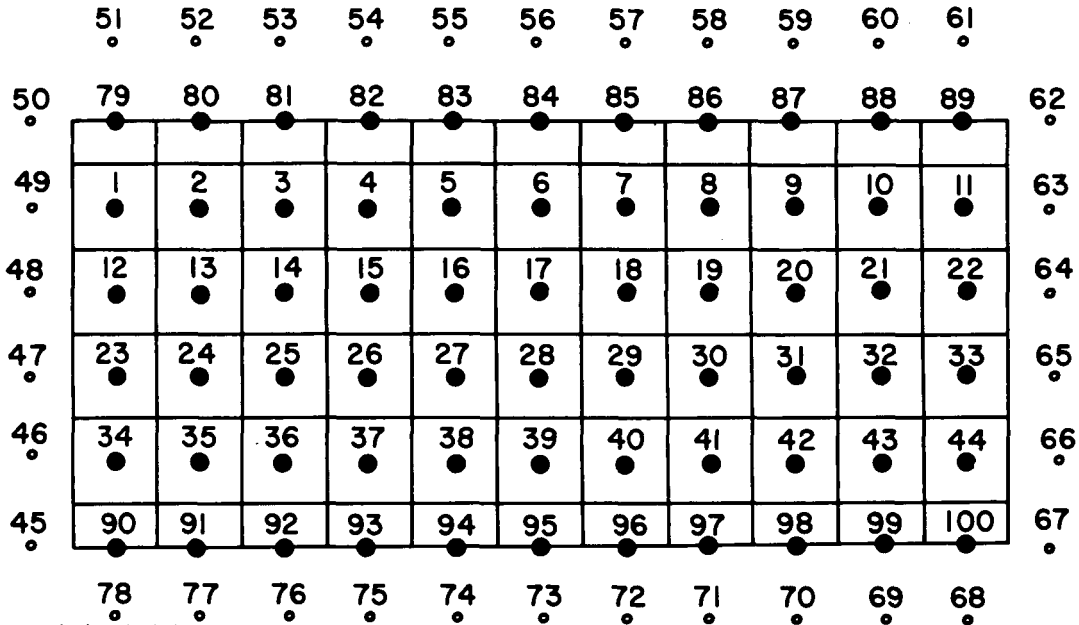

(a) STATIONS FOR FINITE-DIFFERENCE CALCULATIONS OF FREQUENCIES FOR TYPE 1 INTEGRATION. K=44; R=78; T=100 SEE REF. 1

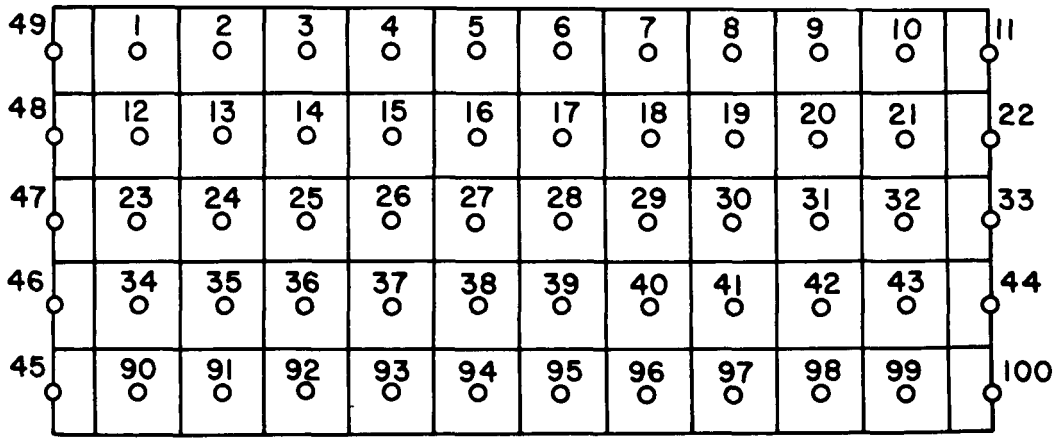

(b) STATIONS FOR TYPE 2 INTEGRATION. SEE REF. 1

NASA

Figure 11.- Planform assumed for panel for calculating frequencies and mode shapes by method of reference 1.